Supporting Information

Environmentally sustainable lithium-ion battery cathode binders based on cellulose nanocrystals

Xingkang Huang,[1,2,*,‡] Haoyang You,[3,‡] Xiaoli Yan,[4,‡] Olaf J. Borkiewicz,[5] Kamila M. Wiaderek,[5] Janan Hui,[6] Mark C. Hersam,[6,7,8] Santanu Chaudhuri,[4,9,*] Stuart J. Rowan,[1,2,3,*] and Junhong Chen[1,2,*]

1. Pritzker School of Molecular Engineering, The University of Chicago, 5640 S. Ellis Ave, Chicago, IL, 60637 USA

2. Chemical Sciences and Engineering Division, Physical Sciences and Engineering Directorate, Argonne National Laboratory, Lemont, Illinois 60439, USA

3. Department of Chemistry, The University of Chicago, Chicago, IL, 60637 USA

4. Department of Civil, Materials, and Environmental Engineering, University of Illinois - Chicago, Illinois, 60439, USA

5. X-ray Science Division, Advanced Photon Source, Argonne National Laboratory, Lemont, IL 60439, USA

6. Department of Materials Science and Engineering, Northwestern University, Evanston, IL 60208, USA

7. Department of Chemistry, Northwestern University, Evanston, IL 60208, USA

8. Department of Electrical and Computer Engineering, Northwestern University, Evanston, IL 60208, USA

9. Applied Materials Division, Advanced Energy Technologies Directorate, Argonne National Laboratory, Lemont, IL, 60439, USA

Experimental section

Materials. *Miscanthus x. Giganteus* (*MxG*) stalks were donated by Prof. Geoff Coates, who grew the grass in Ithaca, New York. Sodium hydroxide (NaOH), acetic acid, and sodium hypochlorite (NaOCl) solution were purchased from Thermo Fisher Scientific. Spinel lithium manganese oxide (LMO), lithium cobalt oxide (LCO), concentrated hydrochloric acid (HCl), sodium chlorite ($NaClO_2$), 2,2,6,6-tetramethylpiperidine 1-oxyl (TEMPO), and sodium bromide (NaBr) were purchased from MilliporeSigma.

Preparation: *MxG*-CNC-OH was isolated from *Miscanthus x. Giganteus* (*MxG*) stalks by NaOH washing, NaClO bleaching, and HCl hydrolysis, and then further oxidized by TEMPO oxidation to obtain *MxG*-CNC-COOH according to a method previously published with slight modification.[1]

Ten grams of ground MxG stems were soaked in 500 mL of deionized water for 4 days. After filtration, two base washes were done by soaking the stems in 150 ml of 2.0 wt.% NaOH solution at 90 °C for 24 hours with a reflux condenser. The fibers were filtered and washed with deionized water after each base wash. The resulting fibers were freeze-dried to yield 6.2 g (62%) of pulp. The pulp was then soaked in 150 mL of 2 wt.% sodium chlorite solution with 6 drops of acetic acid at 70 °C for 2 hours. The resulting suspension was filtered and washed with deionized water and freeze-dried to yield 5.0 g (81%) of white pulp.

To obtain MxG-CNC-OH, the white pulp was hydrolyzed with 150 mL 1M HCl at 70 °C for 18 hours. After washing with deionized water, the MxG-CNC-OH was added to a solution of 0.47 g TEMPO and 6.0 g of NaBr in 390 mL deionized water, in which 100 mL of NaOCl solution was then added. The pH of the mixture was maintained between 10-11 for 4.5 hours. After the reaction was completed, NaCl (10 g) was then added to the mixture and stirred for 10 minutes. 1 M HCl was subsequently added to the reaction to adjust the pH to 6. MxG-CNC-COOH was obtained by centrifuging the mixture, followed by dialysis against deionized water for 3 days, and then freeze-drying. 3.2 g (64%) white fluffy MxG-CNC-COOH was yielded.

The graphene powder was prepared according to a previous publication.[2] Briefly, graphite (MilliporeSigma,+100 mesh) was dispersed in a solution of ethyl cellulose (4 cP, MilliporeSigma) in ethanol (Deacon labs, 200 proof) at a 30:1:20 weight ratio, which was continuously recirculated at a high speed for 48 h in a Silverson 200 L high-shear, inline configuration. The unexfoliated graphite was removed by centrifugation at 6,500 rpm (10,543 g) for 30 min (Avanti J26-XPI centrifuge, JLA 8.1000 rotor, Beckman Coulter). The resulting supernatant of exfoliated graphene nanosheets was flocculated with a 40 g L^{-1} sodium chloride (NaCl, MilliporeSigma) aqueous solution (graphene/ethyl cellulose

dispersion: NaCl solution = 16:9 by weight), which was centrifuged at 7,000 rpm (12,227 g) for 7 min to isolate the graphene/ethyl cellulose flocs and to remove excess polymer binder. The solid floc was washed thoroughly with deionized water using vacuum filtration, and an infrared lamp (150 W, 3 h) was used to obtain the exfoliated graphene/ethyl cellulose dry solids. Graphene content in the resulting solid powder was determined by thermogravimetric analysis (TGA), where the graphene mass fraction was found to be 49.7 % in the exfoliated powder.

Characterization. The morphology of the as-prepared samples was characterized by scanning electron microscopy (SEM) and energy-dispersive X-ray spectroscopy (EDS), performed on a Hitachi S-4700. The atomic force microscopy (AFM) image of *MxG*-CNC-COOH samples was collected by Bruker Multimode 8 AFM with ScanAsyst mode. The sample was prepared by drop casting 100 μL poly-l-lysine solution on a freshly cleaved mica surface, rinsing off with DI water after 3 min, drop casting 100 μL *MxG*-CNC-COOH suspension (0.05 wt. %), rinsing off with DI water after 3 min, then dry overnight at room temperature. The image was analyzed with Gwyddion software.

The carboxylic acid content of the *MxG*-CNC-COOH surface was determined by conductometric titration using an Accumet XL benchtop pH/conductivity meter (Fisher Scientific). Typically, 40 mg of CNC was dispersed in 100 mL of DI water by sonication, and conductivity was adjusted around 300-500 μS cm^{-1} by slowly adding 1 M HCl. Then, 0.01 M NaOH was added slowly (~13 mL/h) using a syringe pump until a pH value of above 11. The conductivities and the pH of the solution were recorded every 15 s to create a conductivity vs. NaOH volume plot. Wide-angle X-ray scattering (WAXS) was conducted with a SAXSLAB GANESHA 300XL using a Cu Kα source (λ = 0.154 nm) at a voltage and current of 40 kV and 40 mA, respectively.[1] Data were collected for 15 minutes at 2θ = 1–33°. Crystallinity was measured by the wide-angle XRD (WXRD) deconvolution method as described in the literature.[3]

High energy synchrotron X-ray powder diffraction was taken at beamline 11-ID-B (λ = 0.1432 Å) at the Advanced Photon Source (APS) of Argonne National Laboratory (ANL). Two-dimensional (2D) images were collected at a nominal sample-to-detector distance of 100 cm using an amorphous silicon area detector. The 2D images were reduced to 1 dimensional diffraction patterns, and Rietveld refinement of the X-ray diffractions was performed simultaneously using GSAS II software. [4]

Computation. Molecular dynamics simulations were conducted using LAMMPS software with ReaxFF pair potential and qeq/reaxff charge equilibrium. [5] The ReaxFF parameters were chosen from a thesis by Reddivari[6] and a journal article by Gomzi, et al. [7] Validation simulations of the force field parameters are conducted on CNC structures (Figure S14-S16). The potential of mean force (PMF) via Jarzynski's equality [8] was evaluated along the user-defined reaction coordinate.[9] The PMF measurements were

normalized based on the area of the contact region of the two groups of atoms.[10] The simulations were conducted with the following conditions: 0.2 femtosecond per step, NVT ensemble at 300 K and 1 atm, steered molecular dynamics (SMD) with approaching constant velocity at 20 m s^{-1} and spring constant k=500,000 kCal mol^{-1}. The CNC-COOH crystal was modeled by 23,706 atoms with 5 × 6 × 7 cellulose units on the (200), (110), and $(1\bar{1}0)$ surfaces, respectively. The carboxylic acid groups only appeared on the (110) and $(1\bar{1}0)$ surfaces.[11]

Preparation of Electrodes and Coin Cells. The charge/discharge performance was characterized by using 2032-type coin cells that were assembled in an argon-filled glove box, with oxygen and moisture content below 1 ppm. Electrodes were prepared by mixing the LMO as the active material, CNC-COOH (or PVDF) as the binder, and carbon black (CB) as a conductor with a weight ratio of 80:10:10 to form a slurry. The resulting slurries were coated onto an Al foil (18-mm in thickness) current collector using the doctor blade method. After drying and pressing, the Al foil was cut into disks (10 mm in diameter) with typical electrode material loadings of ca. 3.5 mg cm^{-2}. To evaluate the full cell performance, the mass loading of the LMO on the electrode was increased to 9.2 mg cm^{-2} using a slurry formula of active material, conductive carbon, and binder with a weight ratio of 93:5:2, to match a graphite anode (approximately 1.15 mAh cm^{-2}), which was from Cell Analysis, Modeling, and Prototyping (CAMP) Facility at ANL. To improve the electronic conductivity, 0.3 wt.% of the CB was replaced by graphene. To achieve environmental sustainability, the graphene was prepared by exfoliating graphite in ethyl cellulose as a bio-based approach, which was described above in detail. As 0.3 wt.% CB was replaced by graphene, ~0.3 wt.% CNC was replaced by the ethyl cellulose. The final slurry formulation consisted of LMO, CB, graphene, CNC-COOH, ethyl cellulose with a mass ratio of 93 : 4.7 : 0.3 : 1.7 : 0.3.

The LCO electrode was prepared using a slurry formula of active material, binder, and conductive carbon with a weight ratio of 95:2:3, as the LCO processes a greater electronic conductivity than the LMO, less carbon additive was needed in the cathode. The mass loading on the LCO electrode was approximately 10.8 mg cm^{-2}. Graphite anode was used as the anode for the full cells; the mass specific capacity ratio of anode to cathode (N/P ratio) was close to 1.1. 1 M $LiPF_6$ dissolved in ethylene carbonate/ethyl methyl carbonate (40:60, v/v) with additives of fluoroethylene carbonate (5 wt. %) and vinylene carbonate (2 wt. %) employed as an electrolyte. The specific current and capacity were calculated based on active materials. To assemble full cell, we adjusted the mass loading on the LCO cathode to let the capacity density match that of the graphite anode (approximately 1.57 mAh cm^{-2}) from CAMP at ANL. The LCO/CNC-COOH||graphite full cells were charged /discharged at a voltage range of 3.0-4.4 V. Note that the voltage upper limit was set as 4.4 V for the LCO/CNC-COOH||graphite full cells because the graphite anodes possess working potential plateaus at 0.5-1.0 V (*vs*. Li^+/Li).

Electrochemistry. The coin cells were tested on a LAND battery tester with a cut-off voltage range between 3 and 4.5 V. Electrochemical impedance spectroscopy (EIS) was tested between 10,000-0.1 Hz with an amplitude of 10 mV on a CHI 660e electrochemical workstation using a three-electrode cell, with the LMO electrode as the working electrode, a lithium disk as the counter electrode, and a lithium ring as the reference electrode.

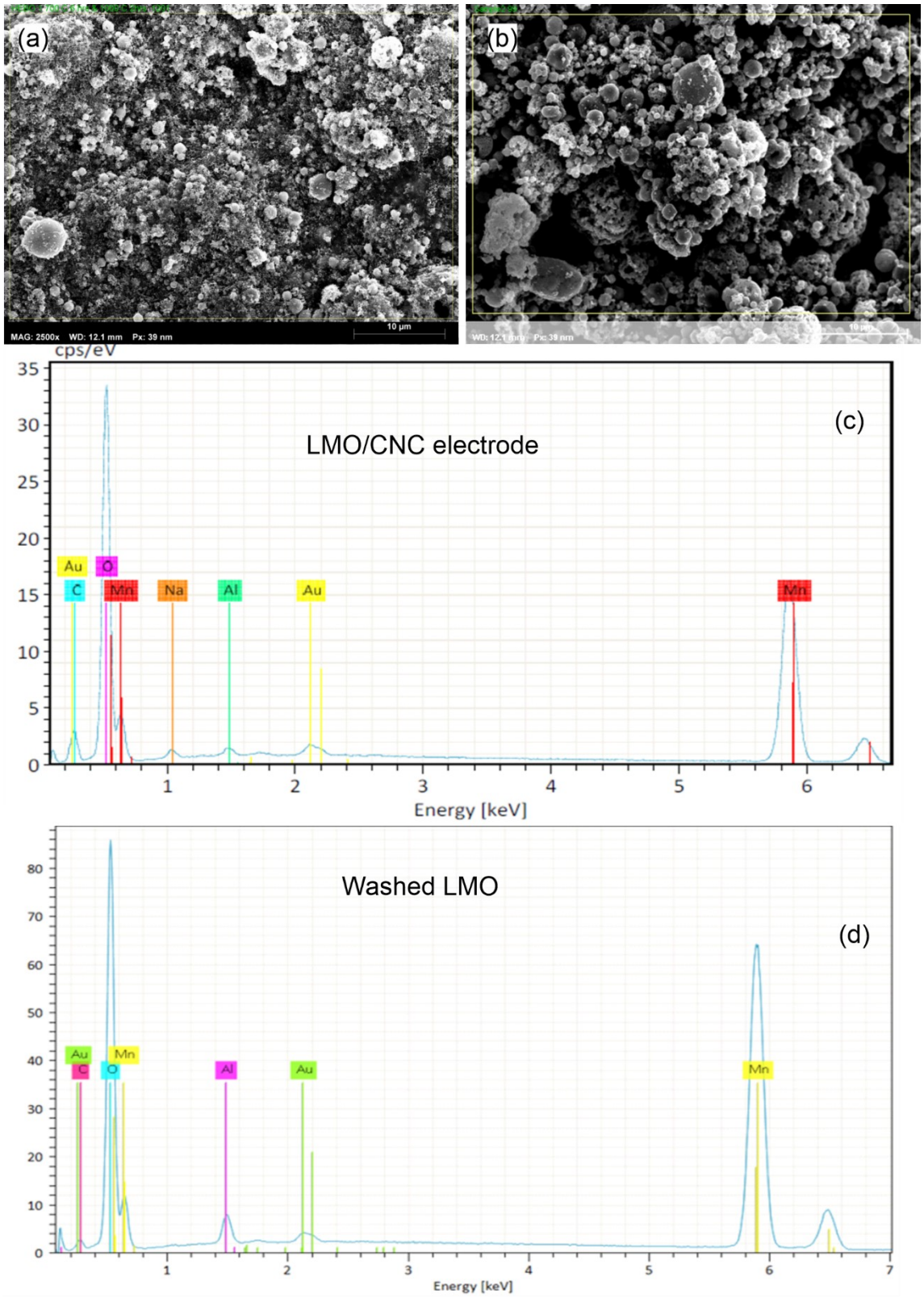

Figure S1. SEM images of (a) fresh LMO/CNC-COOH electrode, and (b) washed LMO, and their corresponding EDS analyses in (c) and (d), respectively. Note that this LMO/CNC-COOH was coated

using LMO:CNC-COOH=90:10 (by weight) without addition of CB, which allows us to observe CNC-COOH contents by C content from EDS analysis.

The LMO can be easily detached from the Al substrate by vortex mixer and sonication in water. Approximately 15 mg LMO was dispersed in 1 mL DI water under sonication for 3 min, followed by centrifuging at 11,000 rpm for 3 min. After being washed 5 times, 0.1 mL DI water was added into the centrifuge tube; the dispersed LMO was dropping cast on an Al tape for EDS analysis. Note that we did not use double-sided C tape to avoid introduction of C. The EDS elemental analysis results for the fresh LMO/CNC-COOH electrode and washed LMO were summarized in Tables S1 and S2, respectively, which indicates the atomic ratio of C/Mn decreased from 0.46 to 0.08 after washing 5 times with water.

Table S1. Elemental analysis results of LMO/CNC-COOH fresh electrode

Element	At. No.	Netto	Mass [%]	Mass Norm. [%]	Atom [%]	abs. error [%] (1 sigma)	rel. error [%] (1 sigma)
Carbon	6	9559	5.15	5.70	12.85	0.75	14.58
Oxygen	8	145580	30.45	33.71	57.02	3.39	11.13
Sodium	11	3969	0.92	1.01	1.19	0.09	9.46
Aluminium	13	3486	0.42	0.47	0.47	0.05	11.16
Manganese	25	158511	51.74	57.28	28.22	1.52	2.94
Gold	79	8787	1.65	1.83	0.25	0.09	5.51
		Sum	90.3186	100	100		

Table S2. Elemental analysis results of DI-water washed LMO

Element	At. No.	Netto	Mass [%]	Mass Norm. [%]	Atom [%]	abs. error [%] (1 sigma)	rel. error [%] (1 sigma)
Carbon	6	7307	1.16	1.26	3.51	0.17	14.50
Oxygen	8	409121	22.25	24.26	50.62	2.32	10.43
Aluminium	13	37358	1.85	2.01	2.49	0.11	5.98
Manganese	25	748008	65.08	70.95	43.12	1.90	2.92
Gold	79	20384	1.39	1.51	0.26	0.08	5.53
		Sum	91.72699	100	100		

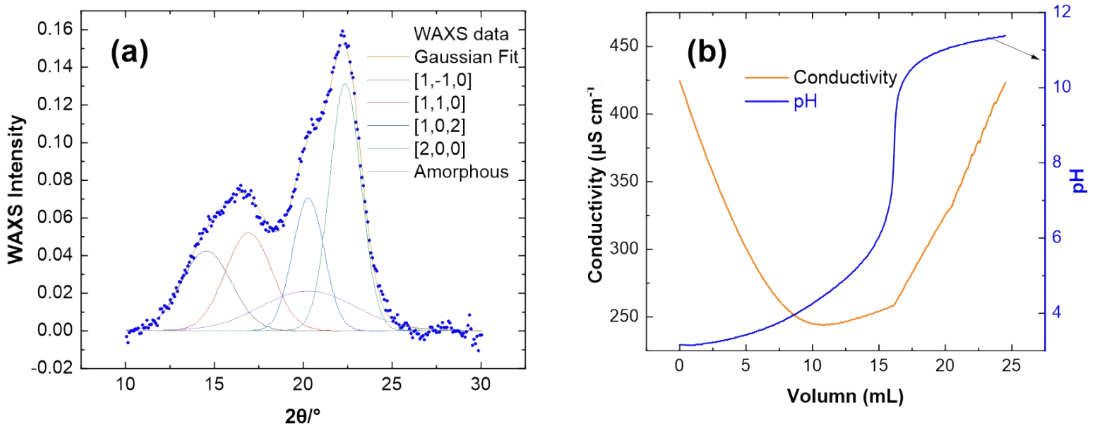

Figure S2. (a) X-ray diffraction pattern and (b) Plot of conductivity and pH value vs. volume of 0.01 M NaOH added to measure the carboxylic acid group content on CNC-COOH.

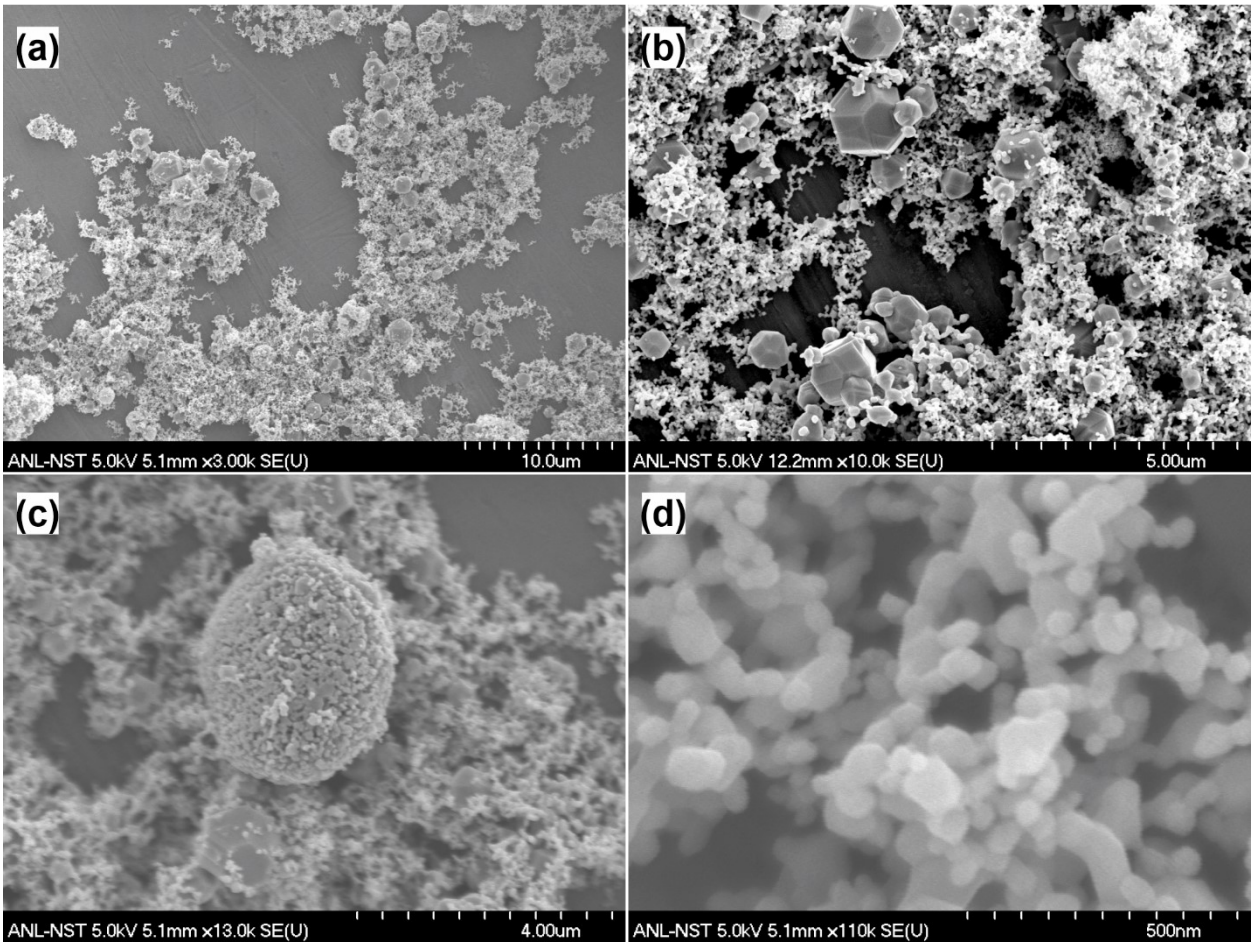

Figure S3. SEM images of the as-received LMO powders at various magnifications, showing two typical morphologies, namely well-defined micron crystals and nanoparticles. Some of the nanoparticles aggregate to spherical secondary particles.

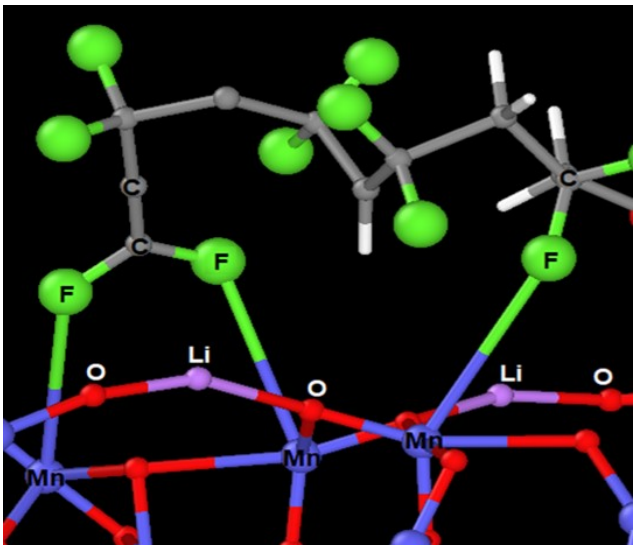

Figure S4. Interaction between Mn in LMO and F in PVDF.

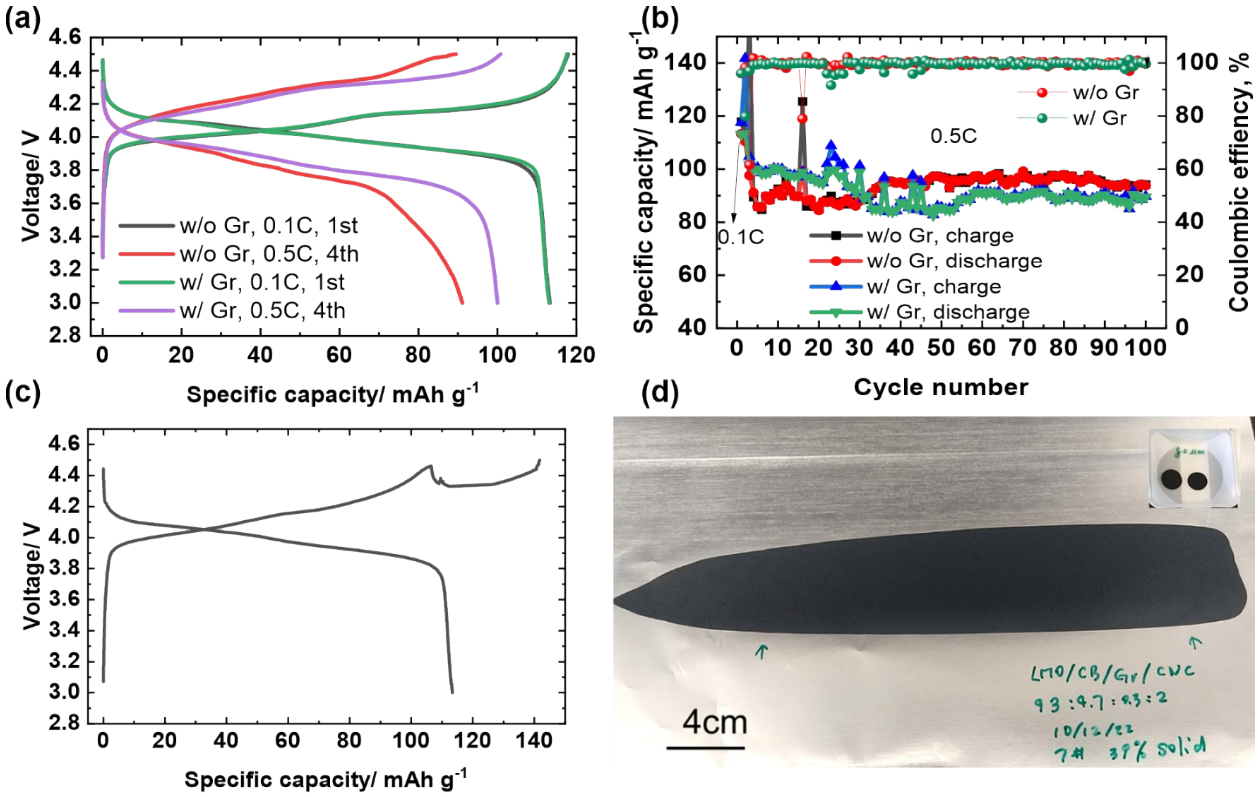

Figure S5. (a) Charge/discharge curves and (b) cyclic performance of the LMO/CNC-COOH electrode with a high mass loading (9.2 mg cm^{-2}), (c) charge/discharge curves of the LMO electrode in a half cell with a high LMO mass loading and the formation of lithium dendrites, and (d) LMO electrode sheet; inset shows two punched electrodes with a diameter of 1 cm.

As shown in Figure S5a, the thick LMO/CNC-COOH electrode delivered a capacity of 113.3 mAh g^{-1} at 0.1 C, which is comparable to that obtained with the lower LMO mass loading electrode (Figure 2b); however, at 0.5 C, the LMO/CNC-COOH showed much higher polarization and lower capacity. Therefore, graphene was used as an additive to improve the electronic conductivity of the LMO cathode. Specifically, graphene/ethyl cellulose powder[3] was dispersed in the CNC-COOH suspension. 0.3 wt.% of CB was replaced by graphene to form slurry, which can be uniformly coated on the Al substrate (Figure S5d). As shown in Figure S5a, the use of 0.3 wt.% of graphene did not change the capacity of the LMO at 0.1 C; however, at 0.5 C, the addition of graphene decreased the polarization and increased the capacity of the LMO, as indicated by their charge/discharge voltage plateaus.

Note that the capacity of the LMO/CNC-COOH electrode showed a lower capacity after 100 cycles in the presence of the graphene, compared with that without graphene (Figure S5a), which, may be related to the lithium electrode of the half cell. With a high mass loading of LMO, it was observed that the voltage suddenly dropped at approximately 4.45 V and then increased to 4.5 V (Figure S5c). This phenomenon is likely due to the formation of lithium dendrites. It was observed that a number of cells with a high mass loading of the LMO exhibited this type of charging curve, a phenomena that was much less frequent in the case of lower mass loading (3.5 mg cm^{-2}) of the LMO (Figure 2b). The continuous growth of lithium dendrites on lithium electrode causes internal shorting, decreasing the voltage of the electrode; on the other hand, the shorting generates heat, breaking down the lithium dendrites, which leads to the voltage increasing again. It is worthy of noting that this phenomenon was not observed in the full cells, consisting of the LMO cathodes and graphite anodes (Figure 2e).

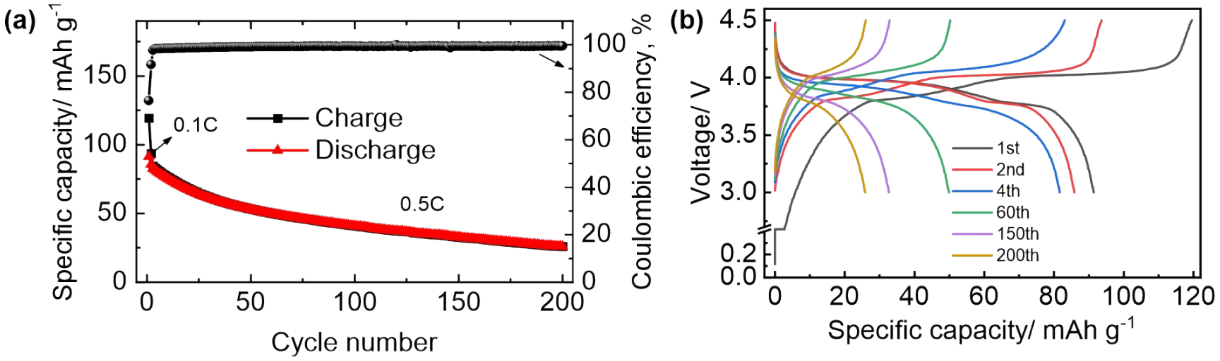

Figure S6. (a) Cyclic performance of LMO/PVDF||graphite full cell and (b) its representative charge/discharge curves.

For fair comparison purpose, we used the same graphite anode with a capacity density of 1.15 mAh cm^{-2}. As the capacity of the LMO cathode is relatively low, it requires relatively high mass loading on the electrode. We control the solid content in the slurry and the coating thickness to achieve the desired mass loading on the electrode. With the CNC-COOH binder, we were able to achieve the active material (LMO) of approximately 9.2 mg cm^{-2}, corresponding to the capacity loading of 1.01 mAh cm^{-2}, which led to an N/P ratio of 1.14. In contrast, with the PVDF binder, with the largest gauge (0.203 mm) that we have, we only could reach the LMO loading of 6.5 mg cm^{-2}, corresponding to 0.71 mAh cm^{-2} and an N/P ratio of 1.62. We were unable to further improve the mass loading on the electrode as the viscosity of the slurry would be too high to coat well on the Al substrate. With a relatively high N/P ratio, it does not require anode fully activated, as less anode is utilized in this case. As shown in Figure S6, the LMO/PVDF||graphite cell delivered an initial capacity of 91.4 mAh g^{-1} at 0.1C and approximately 82 mAh g^{-1} at 0.5 C and remained only 26 mAh g^{-1} after 200 cycles. The poor cyclic performance of the LMO/PVDF||graphite full cell is related to this specific LMO (consisting of microsized and nanosized particles) and the low binder content (2 wt.%). The nanoparticles may require more conductive carbon and binder. In other words, 5 wt.% of CB and 2 wt.% of PVDF might be insufficient for this LMO cathode. It might be possible to improve the cyclic performance of the LMO/PVDF||graphite full cells by optimizing the electrode coating parameters, which is beyond the scope of this study, as we aim to demonstrate the performance of LMO/CNC-COOH||graphite full cells. Therefore, the cyclic performance of the LMO/PVDF||graphite full cell is only for comparison at the most similar conditions to that of the LMO/CNC-COOH||graphite full cell.

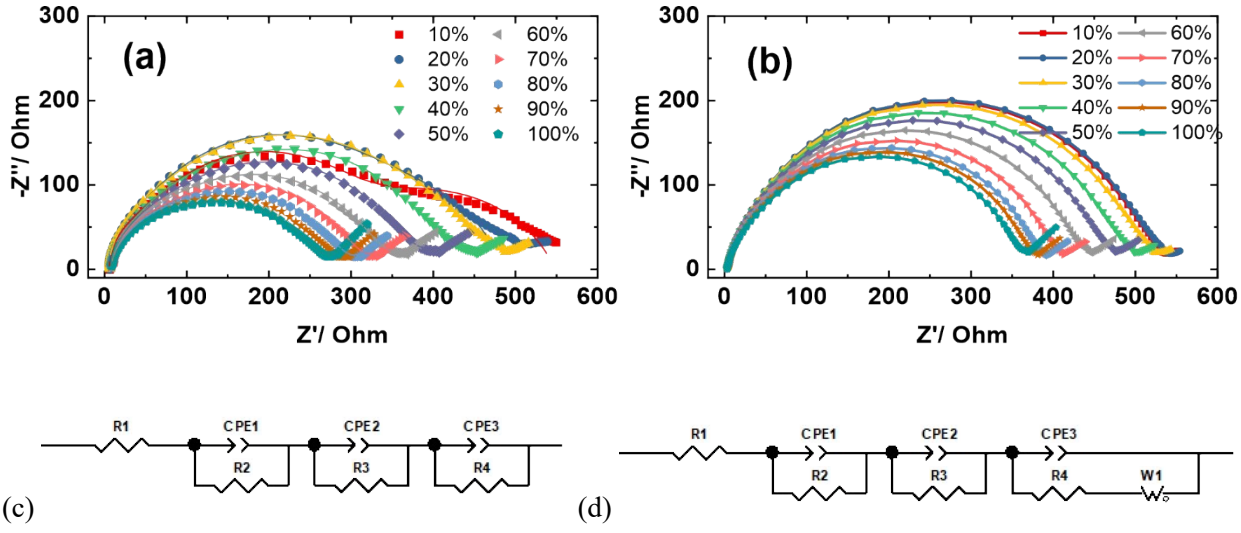

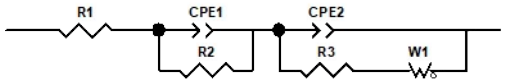

(e)

Figure S7. Nyquist plots of LMO electrodes with (a) CNC-COOH and (b) PVDF binders at various states of charge, and equivalent circuits with (c) three time-constants but no diffusion process (d) three time-constants with diffusion process, and (e) two time-constants with diffusion process.

The fitting results of the LMO with the CNC-COOH binder are shown in Table S3. At low SOCs such as 10%, the Nyquist plot consists of three semi-circles, which was fitted using the equivalent circuit in Figure S7c. R1 and R2 represent the Ohmic resistance and the resistance from the solid-electrolyte interphase. It is not certain for R3 and R4; however, it is likely that both came from the charge transfer resistance of the LMO. Due to the significant size difference (5 mm vs. 30-100 nm in Figure 1b), they might present obvious resistance difference. After SOCs of 40%, significant diffusion was observed at low frequencies; however, at SOC of 40%, when the diffusion process was applied to fit the Nyquist (Figure S7d), the fitting errors were higher than 100% (shown in red in Table S3). It seems that the difference of charge transfer resistance decreased significantly and cannot be differentiated anymore after SOCs of 50% due to their similar time constants. Although this phenomenon is very interesting, it is beyond the current investigation.

Table S3. Fitting results of the LMO cathode with the CNC-COOH binder.

SOC	R1	R1(Err.%)	R2	R2(Err.%)	R3	R3(Err.%)	R4	R4(Err.%)	W1-R	W1-R(Err.%)
10	5.3	2.5	38.6	39.7	253.0	11.7	251.5	15.1	N/A	N/A
20	4.9	4.7	34.4	55.4	166.1	48.7	278.5	32.1	N/A	N/A
30	4.4	8.4	37.0	54.0	128.0	76.1	299.7	35.9	N/A	N/A
40*	7.8	1.4	19.2	78.1	317.2	15.5	64.7	93.2	N/A	N/A
40**	7.4	3.5	9.0	114.7	27.5	91.5	309.2	28.4	267.6	107.7
40***	7.3	2.5	37.7	24.8	229.5	20.7	N/A	N/A	301.7	302.9
50	7.1	2.3	36.8	20.3	291.6	6.2	N/A	N/A	176.3	38.3
60	7.3	2.1	40.9	20.4	262.3	4.3	N/A	N/A	133.3	27.9
70	7.4	1.9	43.6	19.8	234.6	4.5	N/A	N/A	112.8	29.4
80	6.2	6.2	32.0	32.3	238.4	4.9	N/A	N/A	78.8	21.2
90	7.0	3.3	40.4	23.3	214.0	4.9	N/A	N/A	82.1	18.9
100	7.4	1.0	33.3	12.2	208.3	2.1	N/A	N/A	73.0	16.4

Note: * The fitting results were from the three time-constant equivalent circuit without diffusion process (Figure S7c)

** The fitting result was from the three time-constant equivalent circuit with diffusion process (Figure S7d)

*** The fitting result was from the two time-constant equivalent circuit with diffusion process (Figure S7e)

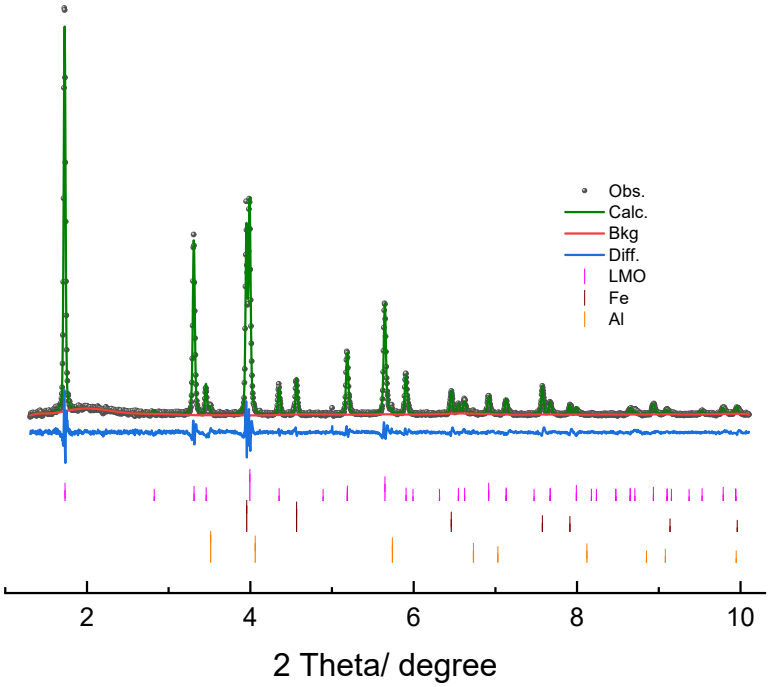

Figure S8. Rietveld refinement of the fresh LMO electrode (the first pattern in Figure 4c).

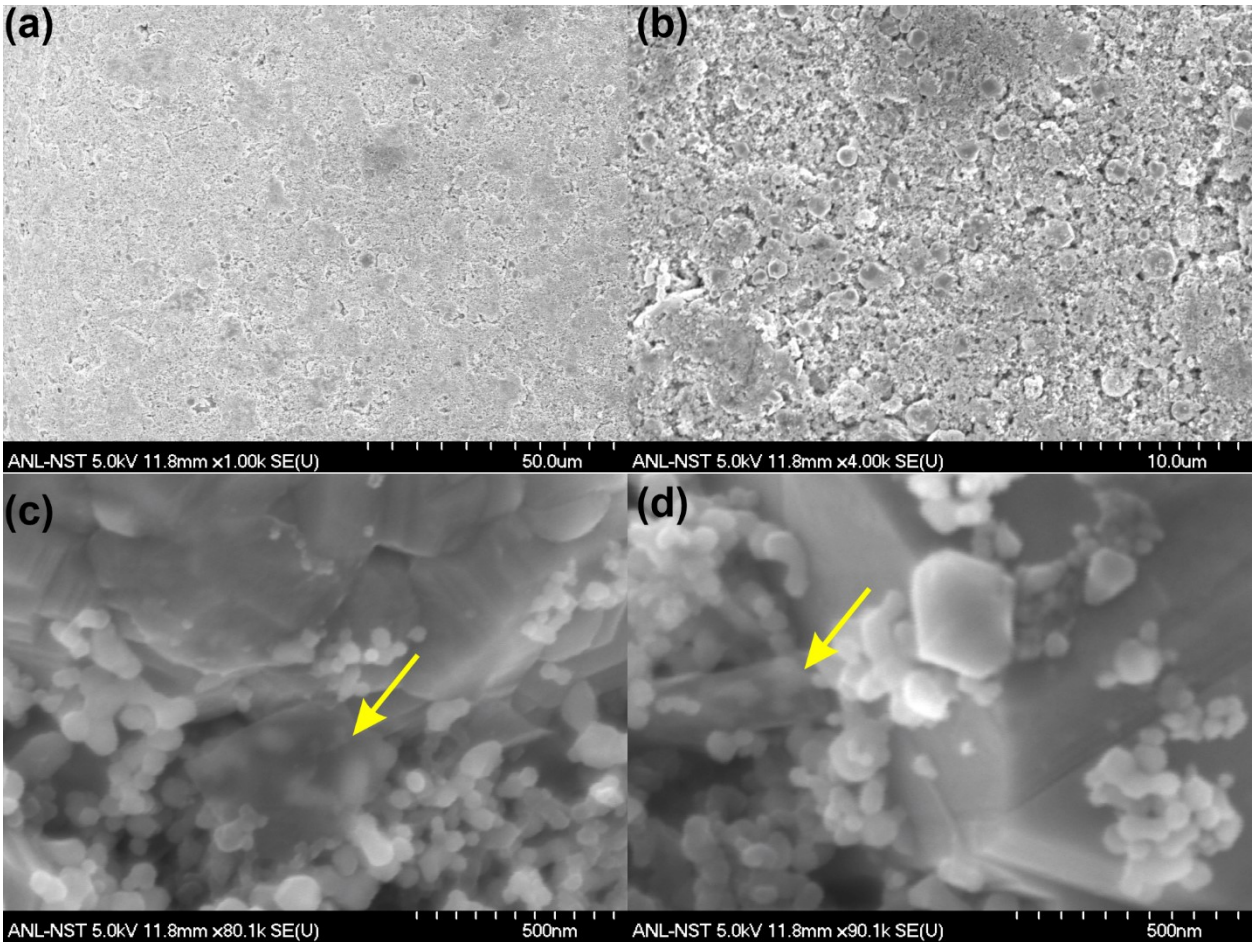

Figure S9. SEM images of cycled LMO electrode at various magnifications. The yellow arrows indicate the graphene sheets.

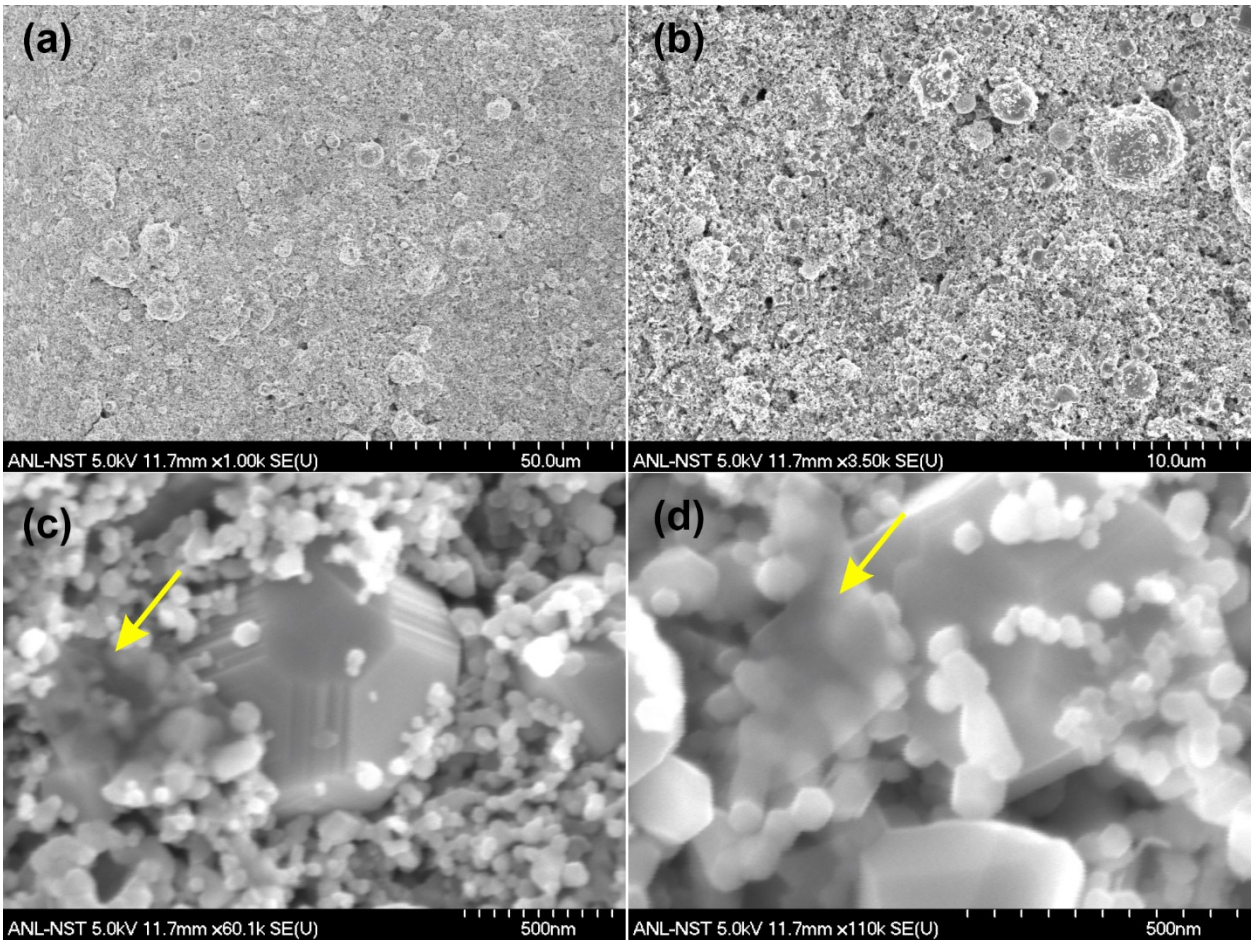

Figure S10. SEM images of fresh LMO electrode at various magnifications. The yellow arrows indicate the graphene sheets.

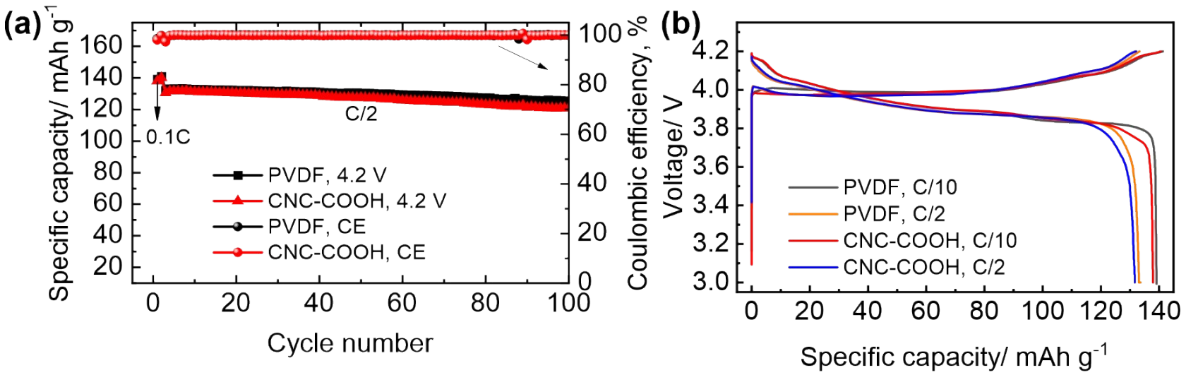

Figure S11. (a) Cyclic performance of LCO/CNC-COOH cathode and (b) its representative charge/ discharge curves with a voltage upper limit of 4.2 V. 1C current was defined as 180 mA g^{-1}.

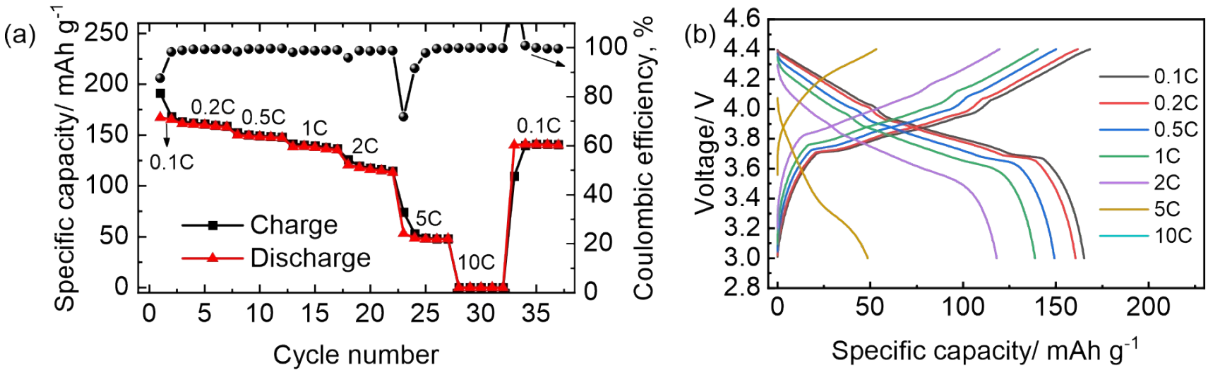

Figure S12. (a) Cyclic performance of LMO/PVDF||graphite full cell and (b) its representative charge/ discharge curves.

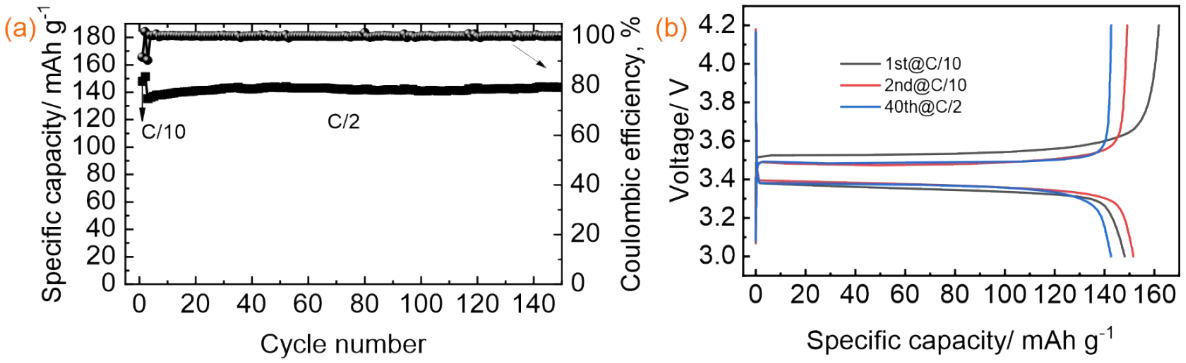

Figure S13. (a) cyclic performance of $LiFePO_4$ cathode using CNC-COOH binder and (b) charge/ discharge curves, in which 1C current was set as 180 mAh g^{-1}. The capacity was approximately 151 mAh g^{-1} at 0.1C and 143 mAh g^{-1} at 0.5C. The ICE was 91.5%. Mass loading on the electrode was approximately 4.7 mg cm^{-2}.

Table S4. Comparison of lattice parameters of CNC

	a (Å)	b (Å)	c (Å)	alpha (°)	beta (°)	gamma (°)
ReaxFF	7.496(62)	7.935(55)	10.701(33)	90.08(48)	90.10(69)	92.9(10)
Experiment [12]	7.784(8)	8.201(8)	10.380(10)	90	90	96.55(5)
relative error	3.70%	3.24%	-3.09%	-0.09%	-0.11%	3.79%

The table shows all simulated lattice parameters are within ±4% of the experimentally measured CNC structure. The equilibrated CNC structure is shown in Figure S14. The ReaxFF equilibration simulation is conducted under 1 atm and 300 K.

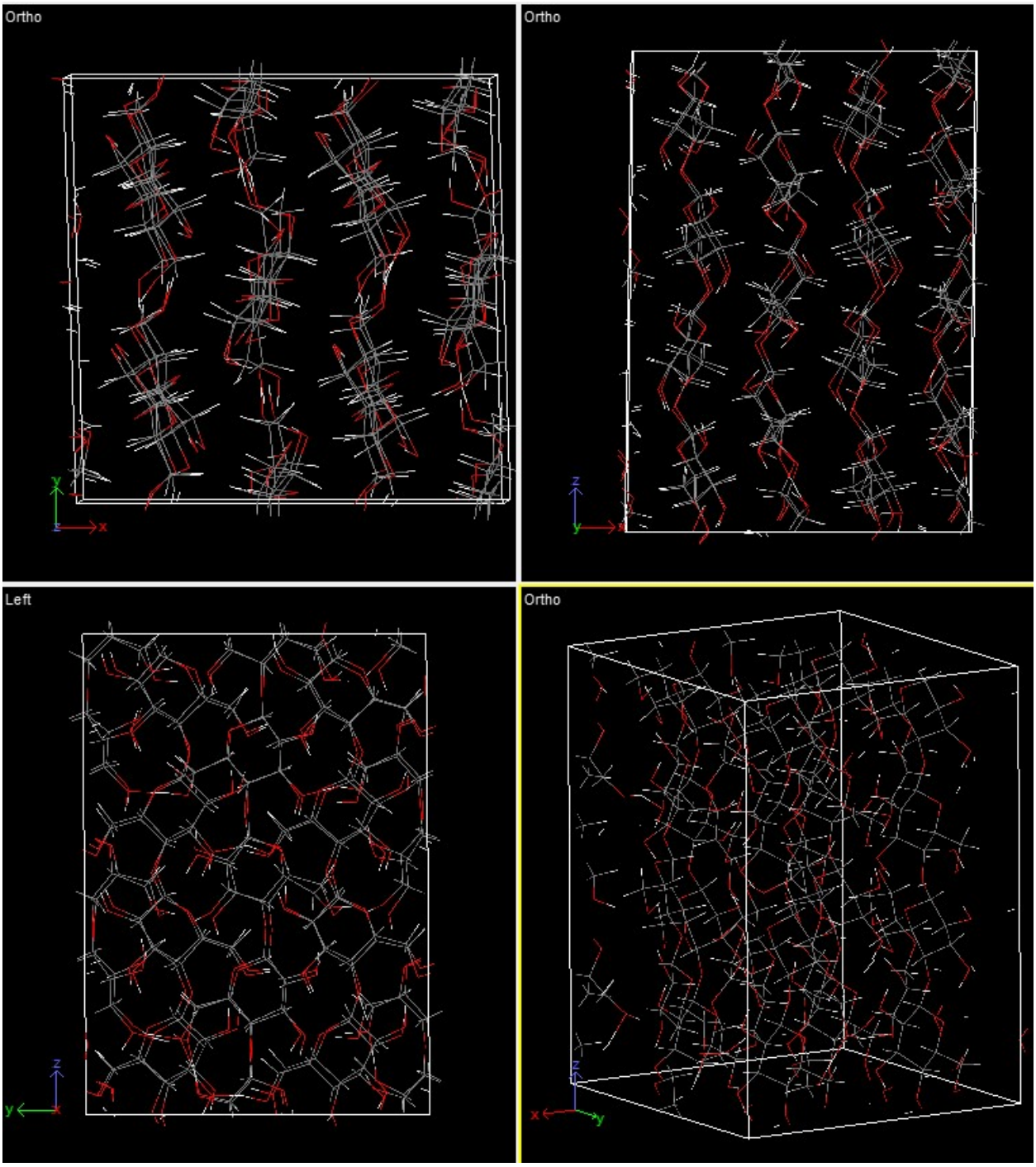

Figure S14. CNC structure with periodic boundary conditions on all three lattice vector directions.

A cellulose nanofibril (CNF) is created with (110), ($1\bar{1}0$) and (200) crystal surfaces. The ReaxFF equilibration simulation is conducted under 1 atm and 300 K. Structures of the CNF before (Figure S15)

and after (Figure S16) simulation are compared. After the relaxation simulation, atom misalignments and distortion are observed on all surfaces of the CNF.

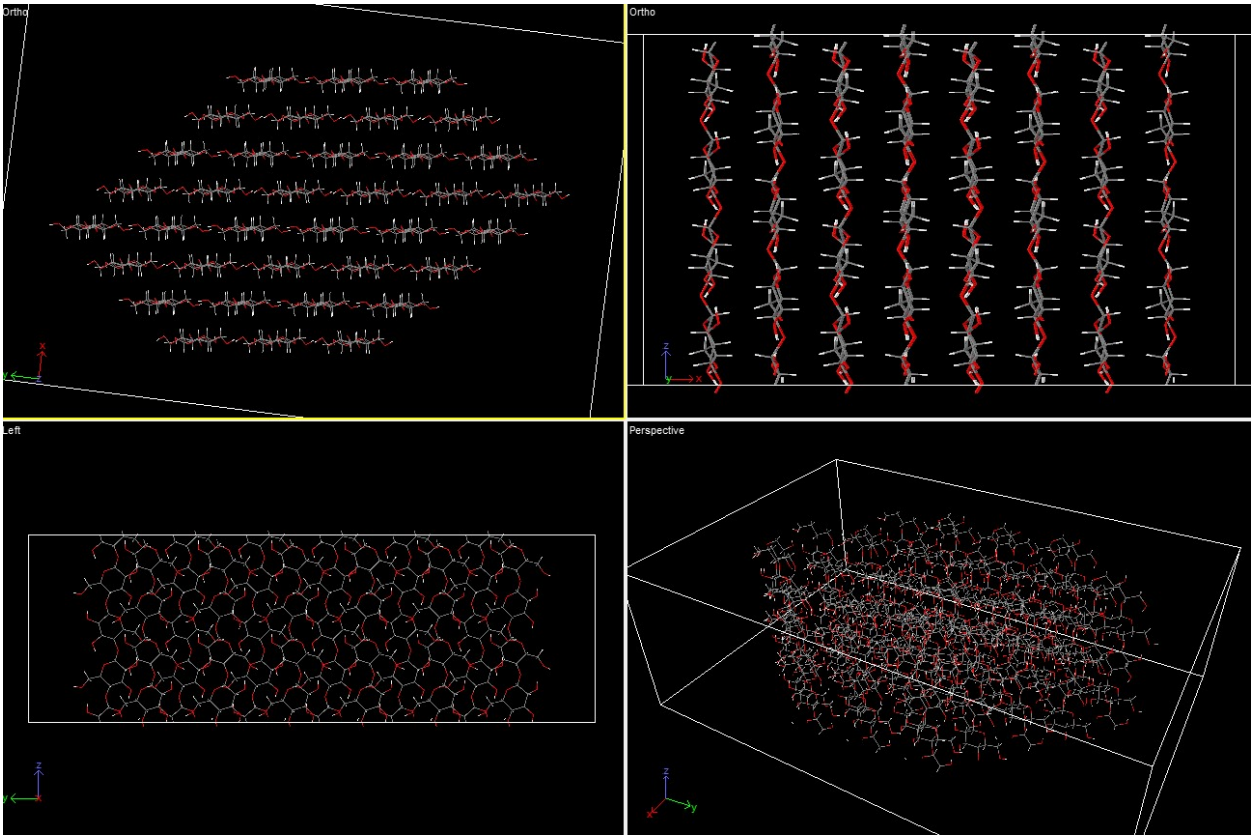

Figure S15. CNC structure before the ReaxFF NPT simulation with periodic boundary condition in the x direction (in the direction of the polymer chain).

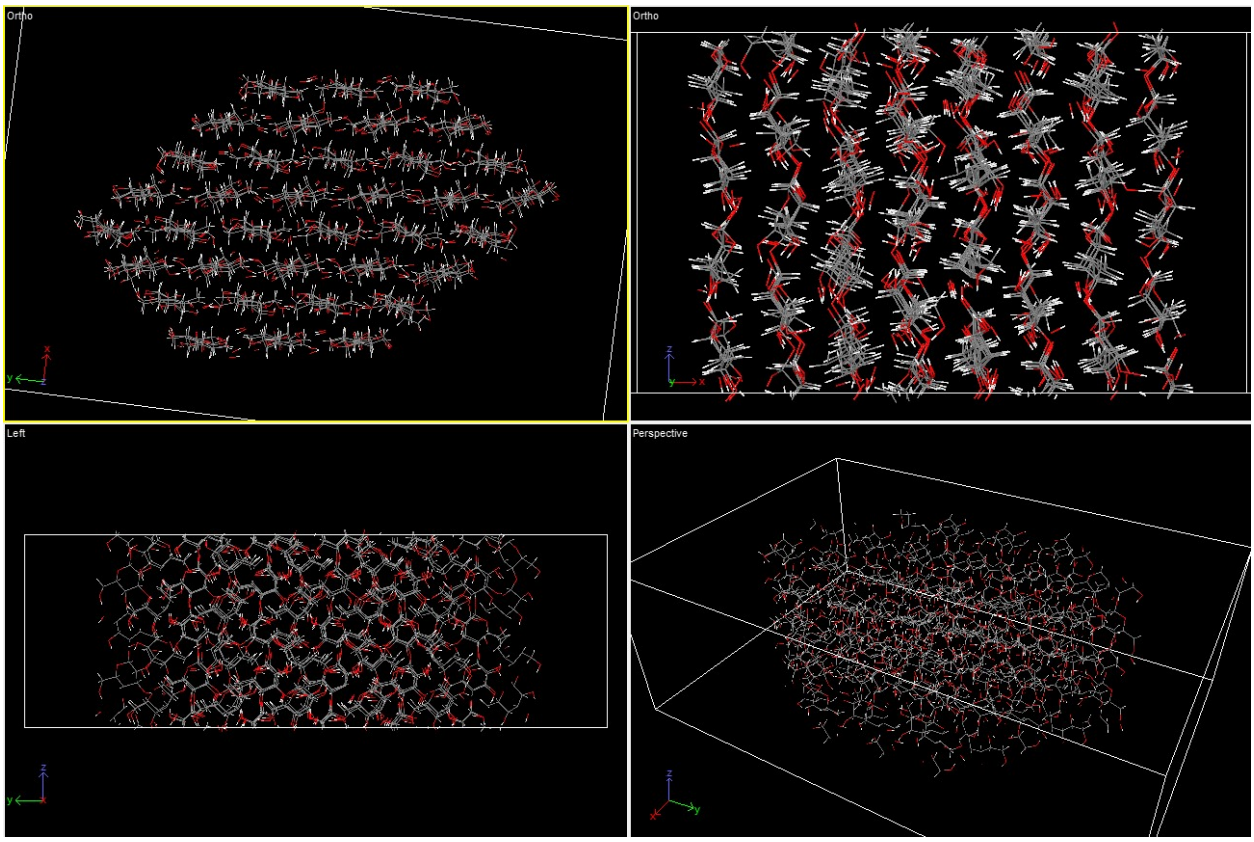

Figure S16. CNC structure after the ReaxFF NPT with periodic boundary condition in the x direction (in the direction of the polymer chain).

References:

[1] E. Cudjoe, M. Hunsen, Z. J. Xue, A. E. Way, E. Barrios, R. A. Olson, M. J. A. Hore, S. J. Rowan, Carbohydr. Polym. 2017, 155, 230.
[2] A. C. M. de Moraes, J. Obrzut, V. K. Sangwan, J. R. Downing, L. E. Chaney, D. K. Patel, R. E. Elmquist, M. C. Hersam, J. Mater. Chem. C 2020, 8, 15086.
[3] S. Park, J. O. Baker, M. E. Himmel, P. A. Parilla, D. K. Johnson, Biotechnol. Biofuels 2010, 3, 10.
[4] B. H. Toby, R. B. Von Dreele, J. Appl. Crystallogr. 2013, 46, 544.
[5] H. M. Aktulga, J. C. Fogarty, S. A. Pandit, A. Y. Grama, Parallel Computing 2012, 38, 245.
[6] S. Reddivari, 2016.
[7] V. Gomzi, I. M. Sapic, A. Vidak, J. Phys. Chem. A 2021, 125, 10649.
[8] C. Jarzynski, Phys. Rev. Lett. 1997, 78, 2690.
[9] S. Park, K. Schulten, J. Chem. Phys. 2004, 120, 5946.
[10] J. Brahmbhatt, X. Bidault, S. Chaudhuri, J. Appl. Phys. 2021, 130.
[11] S. Montanari, M. Rountani, L. Heux, M. R. Vignon, Macromolecules 2005, 38, 1665.
[12] Y. Nishiyama, P. Langan, H. Chanzy, J. Am. Chem. Soc. 2002, 124, 9074.